Stochastic light-cone CTMRG: a new DMRG approach to stochastic models

2003 J. Phys. A: Math. Gen. 36 29

(http://iopscience.iop.org/0305-4470/36/1/303)

INSTITUTE OF PHYSICS PUBLISHING JOURNAL OF PHYSICS A: MATHEMATICAL AND GENERAL

J. Phys. A: Math. Gen. **36** (2003) 29–41 PII: S0305-4470(03)55587-1

Stochastic light-cone CTMRG: a new DMRG approach to stochastic models

A Kemper[1], A Gendiar[2], T Nishino[2], A Schadschneider[1] and J Zittartz[1]

[1] Institut für Theoretische Physik, Universität zu Köln, 50937 Köln, Germany
[2] Department of Physics, Faculty of Science, Kobe University, Rokkodai 657, Japan

E-mail: kemper@thp.uni-koeln.de, gendiar@phys.sci.kobe-u.ac.jp, nishino@phys.sci.kobe-u.ac.jp and as@thp.uni-koeln.de

Received 4 November 2002
Published 10 December 2002
Online at stacks.iop.org/JPhysA/36/29

Abstract

We develop a new variant of the recently introduced stochastic transfer matrix DMRG which we call stochastic light-cone corner-transfer-matrix DMRG (LCTMRG). It is a numerical method to compute dynamic properties of one-dimensional stochastic processes. As suggested by its name, the LCTMRG is a modification of the corner-transfer-matrix DMRG, adjusted by an additional causality argument. As an example, two reaction–diffusion models, the diffusion–annihilation process and the branch–fusion process are studied and compared with exact data and Monte Carlo simulations to estimate the capability and accuracy of the new method. The number of possible Trotter steps of more than 10^5 shows a considerable improvement on the old stochastic TMRG algorithm.

PACS numbers: 02.50.Ey, 64.60.Ht, 02.70.−c, 05.10.Cc

1. Introduction

The density-matrix renormalization group (DMRG), developed by White in 1992 [1], is one of the most precise numerical algorithms for the investigation of low-dimensional strongly correlated systems. Originally, the DMRG was introduced to compute the ground state and low-energy spectrum of a quantum Hamiltonian H. Meanwhile, there are a number of variants using the basic DMRG idea of numerical renormalization in other physical fields [2]. Important progress was made by applying the DMRG to the transfer matrix of 2D classical systems [3], a method known as transfer matrix DMRG (TMRG). This even allows us to analyse the thermodynamics of 1D quantum systems [4] by mapping the partition function to a 2D classical model using a Trotter–Suzuki decomposition [5]. A highly efficient realization of a TMRG algorithm, which uses corner transfer matrices (CTMs), was proposed in [6] and is called corner-transfer-matrix DMRG (CTMRG).

An upcoming new application field of the DMRG algorithm is 1D stochastic systems. The dynamics of such models are described by a master equation which has the form of a Schrödinger equation with a 'stochastic' Hamiltonian H [7, 8]. The DMRG algorithm can be used for computing the stationary limit of the stochastic process, which corresponds to the ground state of H. In contrast to quantum systems H is, in general, not Hermitian since there is genuinely no detailed balance. Carlon *et al* [9] first applied the stochastic DMRG algorithm to various reaction–diffusion models and discussed in detail the influence of non-Hermitian operators on the numerics.

An alternative approach to stochastic models using a TMRG algorithm was proposed in [10]. In complete analogy with quantum systems, the dynamics of 1D stochastic models can be mapped to a 2D classical model. Therefore, it was quite natural to apply the TMRG to the corresponding 'stochastic' transfer matrix. Even though this so-called stochastic TMRG is similar to the quantum case in many respects, some important differences appear. Enss and Schollwöck [11] discussed in detail properties of the stochastic transfer matrix focussing on the choice of the density matrix. Unfortunately, the stochastic TMRG shows an unsatisfactory convergence caused by inherent numerical problems which are related to the structure of the stochastic transfer matrix.

The present work proposes a new approach to analyse the dynamics of stochastic problems, a method which we refer to as stochastic light-cone CTMRG (LCTMRG). As suggested by its name, the LCTMRG combines ideas of the stochastic TMRG and CTMRG algorithms, adjusted by a causality argument which demands a number of modifications for an adaption of the CTMRG to stochastic problems. We show that the LCTMRG is a considerable improvement of the stochastic TMRG with respect to numerical stability and performance.

2. Stochastic models

Stochastic models have gained great interest in statistical physics. They are used not only in physical but also in many interdisciplinary research fields to describe processes far away from thermal equilibrium [8, 12]. The bandwidth of applications reaches from the description of social behaviour and biological processes to traffic flow (see, e.g., [13, 14]). Typically, stochastic models start from an initial state which evolves in time according to (local) probabilistic rules.

In the present work we focus on one-dimensional stochastic problems. We consider a chain of length L, where each site s_i can either be occupied by a particle ($s_i = 1$) or empty ($s_i = 0$). In stochastic physics one is interested in the dynamic evolution of a probability distribution $P(t)$ of states. $P(t)$ can be denoted as a vector

$$|P(t)\rangle = \sum_{s\in\mathcal{S}} P_s(t)|s\rangle \tag{1}$$

where $P_s(t)$ is the probability of finding the chain in the configuration

$$s = (s_1, s_2, \ldots, s_L) \in \mathcal{S} = \{0, 1\}^{\otimes L}. \tag{2}$$

Depending on the type of dynamics, $|P(t)\rangle$ can evolve in continuous or discrete time. Assuming continuous dynamics, stochastic processes can be described by a master equation

$$\partial_t|P(t)\rangle = -H|P(t)\rangle. \tag{3}$$

H is called a 'stochastic Hamiltonian' [7, 8] because (3) has the form of a Schrödinger equation in imaginary time. The matrix elements are given by

$$\langle s|H|\tilde{s}\rangle = -w(\tilde{s} \to s) + \delta_{s,\tilde{s}} \sum_{s'\in\mathcal{S}} w(s \to s') \tag{4}$$

where $w(\tilde{s} \to s)$ denote the probabilistic rates of the transition $\tilde{s} \to s$. Although the master equation (3) suggests a close analogy with quantum systems, as an important difference the stochastic Hamiltonian H is in general *not* Hermitian. A formal solution of (3) is given by

$$|P(t)\rangle = \mathrm{e}^{-tH}|P(0)\rangle \tag{5}$$

where $|P(0)\rangle$ denotes the initial probability distribution at $t = 0$. Obviously, the stationary limit $|P(\infty)\rangle$ is a (right) eigenvector of H with eigenvalue 0.

Stochastic models can show a rich phase diagram and interesting critical phenomena [15]. The simplest situation is an absorbing phase transition [12] into an empty state $|00\cdots0\rangle$. Introducing the occupation number operator n_j of site j, the average local density of particles

$$n(t) = \langle 1|n_j|P(t)\rangle \qquad \text{with} \quad \langle 1| := \sum_{s\in\mathcal{S}}\langle s| \tag{6}$$

(with arbitrary j due to translational invariance) is an order parameter that distinguishes the phases: all particles can either vanish ($n(\infty) = 0$) and the system falls into the (absorbing) state $|P(\infty)\rangle = |00\cdots0\rangle$, or a certain number of particles stay 'active' ($n(\infty) \neq 0$). In the critical region $n(t)$ evolves according to a power law whereas a non-critical behaviour is characterized by an exponential decay:

$$n(t) - n(\infty) \sim \begin{cases} \mathrm{e}^{-t/\tau} & \text{non-critical} \\ t^{-\alpha} & \text{critical.} \end{cases} \tag{7}$$

Like quantum systems, stochastic processes show universal behaviour at criticality. The most prominent universality class, which is typical for phase transitions to an absorbing state, is the directed percolation class (DP) [16]. But, in general, non-equilibrium phase transitions are by far not so well understood as those in equilibrium physics.

3. Stochastic transfer-matrix DMRG

3.1. The stochastic transfer matrix

We focus on the calculation of the dynamic evolution of the local density

$$n(t) = \langle 1|n\,\mathrm{e}^{-tH}|P(0)\rangle \tag{8}$$

of a stochastic process in the thermodynamic limit $L \to \infty$ and assume that H consists of local 'stochastic interactions'

$$H = \sum_i h_{i,i+1}. \tag{9}$$

As in the conventional quantum TMRG algorithm [4], the stochastic system is first mapped to a 2D statistical model by using a Trotter–Suzuki decomposition [5] of (8). The resulting classical 2D lattice [10, 11] is shown in figure 1(*a*) where local plaquette interactions are given by

$$(\tau)^{l_1 l_2}_{r_1 r_2} = \langle l_2 r_2|\,\mathrm{e}^{-\Delta t h}|l_1 r_1\rangle = \quad \text{with} \quad l_i, r_i \in \{0, 1\}. \tag{10}$$

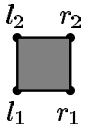

Thus, the spatial dimension L of the stochastic process is expanded by a virtual Trotter dimension $M = t/\Delta t$ which corresponds to the time direction and is split into (discrete) steps of size Δt. Δt has to be chosen sufficiently small to obtain a good approximation of $n(t)$. Formally, the Trotter decomposition becomes exact for $\Delta t \to 0$. As we measure the local

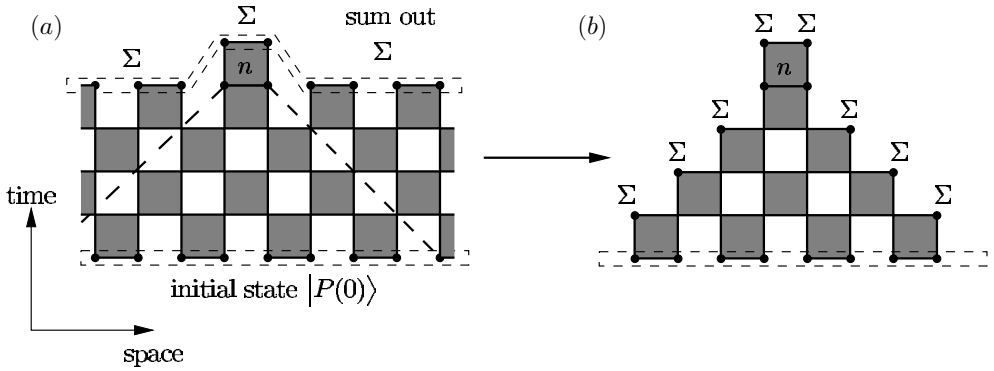

Figure 1. (*a*) Trotter–Suzuki decomposition of $2\Delta t$ time steps. The resulting 2D lattice consists of local plaquette interactions τ and is infinitely extended in the space direction. The dimension of the time direction is finite and the boundary conditions are fixed by $\langle 1|$ and $|P(0)\rangle$. (*b*) Reduction of the 2D lattice to a triangle structure. All other plaquettes trivialize due to (13).

density $n(t)$ at finite time t, but in the thermodynamic limit $L \to \infty$ of the stochastic chain, the space dimension of the 2D lattice is infinite, whereas the Trotter dimension is finite. Note that in contrast to the quantum TMRG the boundary conditions are fixed in the Trotter direction and given by the vectors $\langle 1|$ and $|P(0)\rangle$ (cf figure 1(*a*)).

In complete analogy with the quantum case one can apply a TMRG algorithm to the 2D lattice [10, 11]. Using column transfer matrices, shown here pictorially for the example of figure 1(*a*),

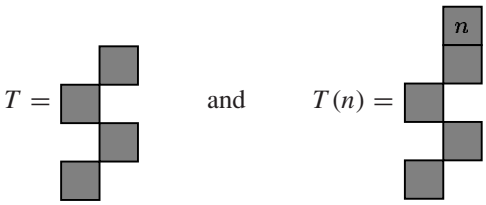

(11)

the local density $n(t)$ for the thermodynamic limit $L \to \infty$ can be calculated by

$$n(t) = \langle \psi_L | T(n) | \psi_R \rangle. \tag{12}$$

$|\psi_{R/L}\rangle$ labels the leading right/left eigenvector of T, having the eigenvalue 1 [11]. The stochastic TMRG algorithm is used for computing $|\psi_{R/L}\rangle$ and $T(n)$ for successively increasing Trotter numbers M. Unfortunately, various computations show numerical problems that limit $M \sim 10^2$ [10, 11], which is far from enough to compete with other methods such as Monte Carlo simulations (MCS).

Here we propose a different TMRG algorithm based on corner transfer matrices (CTM). Such a corner-transfer-matrix DMRG algorithm (CTMRG) is known to be numerically more stable and faster than TMRG [6]. Before we explicitly construct these CTMs for the stochastic case, we discuss some physical properties of the 2D lattice relevant for the development of the new algorithm.

Due to probability conservation we have $\langle 1| \mathrm{e}^{-\Delta t h} |s\rangle = 1$ for any state $|s\rangle$. Thus, τ trivializes by summing out the 'future' indices, i.e.

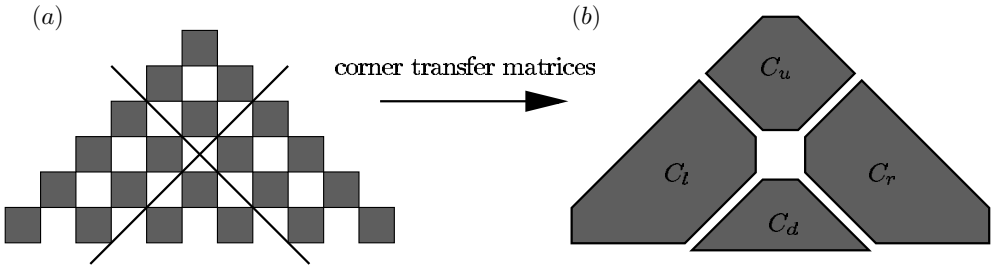

Figure 2. Construction of corner transfer matrices. (*a*) The lattice is split into four parts. (*b*) Schematic plot of the corner transfer matrices C_u, C_d, C_l and C_r evolving from (*a*).

$$\forall l_1, r_1: \quad \sum_{l_2 r_2} (\tau)^{l_1 l_2}_{r_1 r_2} = 1 \qquad \Sigma l_2 \;\; \Sigma r_2 \;\; l_1 \;\; r_1 \;\; = 1. \tag{13}$$

The effect of (13) on the 2D lattice is discussed in detail in [11]. For the computation of $n(t)$ it is found that a huge number of plaquette interactions can be omitted, because they 'trivialize'. The remaining non-trivial plaquettes form a 2D lattice of *finite* dimension which is shown in figure 1(*b*). The trivialization process can easily be understood by a causality argument: only a 'light cone' of plaquette interactions can influence the site where the local density is measured.

We now construct a CTMRG algorithm which genuinely fits the triangle structure of the 2D lattice. As shown in figure 2, four cuts are set to separate the lattice into four parts. The cuts are somewhat native to our model, because they form the boundaries of the 'future' and 'past light cone' of the centre point of the triangle. The four parts

$$(C_l)^{\bar{n}_s}_{n_s} = \qquad (C_r)^{\bar{n}_s}_{n_s} = \tag{14}$$

$$(C_d)^{\bar{n}_s}_{n_s} = \qquad (C_u)^{\bar{n}_s}_{n_s} = \tag{15}$$

are interpreted as CTMs whereby n_s and $\bar{n}_s$ label block spins. We next show how these CTMs can be treated within a CTMRG algorithm analogous to, e.g., [6]. However, a number of modifications are necessary to adapt the CTMRG to the light cone of plaquettes. Hence, we call this CTMRG variant light-cone CTMRG (LCTMRG).

3.2. The light-cone-CTMRG algorithm

In a CTMRG algorithm the CTMs are enlarged sequentially by adding transfer matrices (TMs) to each cut. We first define the TMs in a pictorial way

$$(T_{ld})^{\bar{n}_s \bar{s}}_{n_s s} = \qquad (T_{rd})^{\bar{n}_s \bar{s}}_{n_s s} = \tag{16}$$

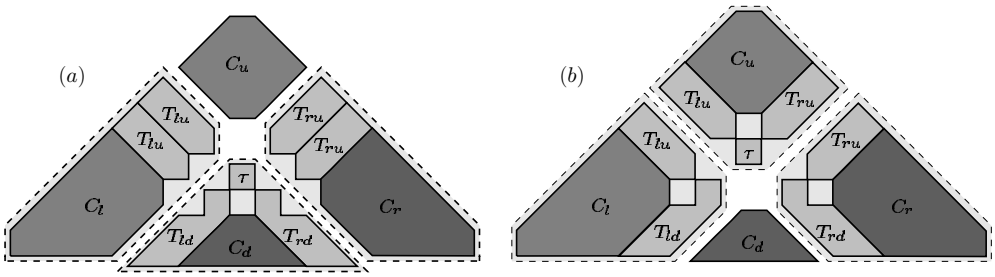

Figure 3. Extension of the CTMs by adding diagonal TMs. In (*a*) the lower part of the triangle is enlarged whereas in (*b*) the extension is performed to the upper part. In the LCTMRG algorithm the upper and lower extensions are done alternately, so that all CTMs grow step by step.

$$(T_{lu})^{\bar{n}_s}_{n_s s} = \quad (T_{ru})^{\bar{n}_s}_{n_s s} = \quad . \tag{17}$$

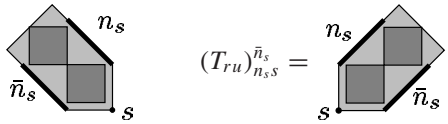

The bullets represent single-spin sites $s, \bar{s}$ and the spins $n_s, \bar{n}_s$ marked with bars will become renormalized block spins in the DMRG algorithm. Exemplarily, (16) and (17) show TMs which are used to enlarge the triangle lattice of figure 2(*a*).

Figure 3 demonstrates graphically how the TMs are used to enlarge the CTMs, whereby CTMs and TMs are 'jointed' by summing out the adjacent indices (similar to a matrix multiplication). Due to the exotic geometry of the lattice we have to distinguish between an upper and lower extension step depending on whether C_u or C_d should be enlarged. In our LCTMRG algorithm both extension steps are implemented alternately. That way all CTMs grow step by step with the crossing point of the cuts always situated at the centre of the triangle. After each extension step the CTMs have to be renormalized by a density-matrix projection (cf section 3.3).

The local density $n(t)$ can be obtained using C_d, T_{ld} and T_{rd}

$$n(t) = \quad . \tag{18}$$

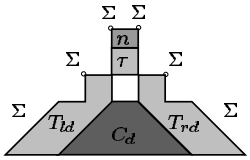

It is important to note that $n(t)$ is computed at the centre of the triangle lattice. Here, influences of boundary effects are expected to be smallest. In terms of a DMRG algorithm, the CTMs C_l, C_r and C_u act as an 'environment' of the 'system' C_d.

3.3. The choice of the density matrix

The key problem is to find a reasonable density matrix projection for the renormalization of the CTMs after each extension step. We exemplify the construction of the density matrix by looking at figure 3(*a*). Here, one block spin and two spins of C_d, C_l and C_r have to be renormalized into one block spin. The construction of the optimal density-matrix projection is now discussed in detail.

First, we define four vectors:

$\left(\psi_R^R\right)^{\bar{n}_s}_{n_s,s_1,s_2} =$ 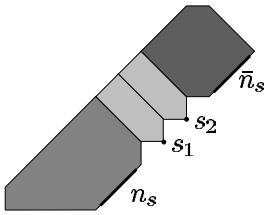

$\left(\psi_L^R\right)^{\bar{n}_s}_{n_s,s_1,s_2} =$ 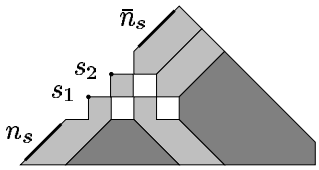

(19)

$\left(\psi_R^L\right)^{\bar{n}_s}_{n_s,s_1,s_2} =$ 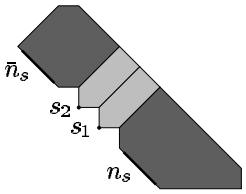

$\left(\psi_L^L\right)^{\bar{n}_s}_{n_s,s_1,s_2} =$ 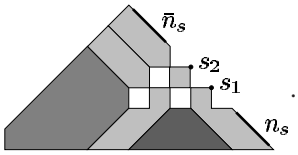

.

(20)

The block spin $\bar{n}_s$ belongs to the environment, s_1, s_2 and n_s to the system block. Note that these vectors approximate the left and right eigenvectors of the leading eigenvalue of diagonal TMs

$T_R =$ 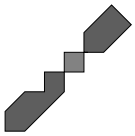 and $T_L =$ 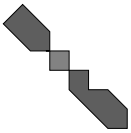 (21)

which have a different shape compared to the stochastic TMs used in the stochastic TMRG [10, 11]. As ψ_R^x and ψ_L^x ($x = L, R$) do not have to be computed by any expensive diagonalization routine as in TMRG, the LCTMRG algorithm is much faster.

ψ_R^x and ψ_L^x are used for constructing a reduced density matrix for each of the two cuts. The most generic choice would be a symmetric density matrix

$$\rho_x^{[1]} = \mathrm{tr}_{\bar{n}_s}\left(\left|\psi_L^x\right\rangle\left\langle\psi_L^x\right| + \left|\psi_R^x\right\rangle\left\langle\psi_R^x\right|\right) \tag{22}$$

which was also used in [9–11]. Here, $\mathrm{tr}_{\bar{n}_s}$ denotes the partial trace over $\bar{n}_s$. $\rho_x^{[1]}$ produces a reduced system block basis which optimally approximates ψ_L^x and ψ_R^x [9]. However, one can easily prove that ψ_R^x is trivially given by

$$\left(\psi_R^x\right)^{\bar{n}_s}_{n_s,s_1,s_2} = 1 \qquad \text{for all} \quad n_s, s_1, s_2, \bar{n}_s \tag{23}$$

which follows directly from the trivialization process (13). Obviously, ψ_R^x is not very useful for constructing a density matrix, because

$$\mathrm{tr}_{\bar{n}_s}|\psi_R\rangle\langle\psi_R| = |1_s\rangle\langle 1_s| \qquad \text{with} \quad (1_s)_{n_s,s_1,s_2} = 1 \tag{24}$$

reduces to a trivial projector which does not correlate system and environment block. Hence, we omitted ψ_R^x and tested the density matrix

$$\rho_x^{[2]} = \mathrm{tr}_{\bar{n}_s}\left|\psi_L^x\right\rangle\left\langle\psi_L^x\right| \tag{25}$$

which led to much better results (cf section 4.2). An asymmetric choice

$$\rho_x^{[3]} = \mathrm{tr}_{\bar{n}_s}\left|\psi_R^x\right\rangle\left\langle\psi_L^x\right| \tag{26}$$

of the density matrix performs worst. As

$$\langle n_s', s_1', s_2'|\rho_x^{[3]}|n_s, s_1, s_2\rangle = \sum_{\bar{n}_s} \left(\psi_L^x\right)^{\bar{n}_s}_{n_s,s_1,s_2} \tag{27}$$

is independent of n_s', s_1', s_2', the density matrix $\rho_x^{[3]}$ has rank one and represents a pure projector.

A physical explanation for the choice of $\rho_x^{[2]}$ can be given in terms of the light-cone picture of section 3.1. The trivial vector $\left|\psi_R^x\right\rangle$ is a superposition of all feasible states which means that at each cut no further information about the 'future' is available. Not surprisingly, the system and environmental part of the cut are uncorrelated which is expressed by a trivial density-matrix projection of $\mathrm{tr}_{\bar{n}_s}\left|\psi_R^x\right\rangle\left\langle\psi_R^x\right|$. Only the physics of the past, the information of which is carried by $\left|\psi_L^x\right\rangle$, correlates system and environment indices.

3.4. Some technical aspects

We briefly discuss some implementation details of the LCTMRG algorithm.

The first TMRG step should start with the following configuration

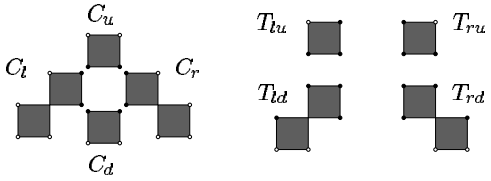

of transfer matrices. This corresponds to the time $t = 1.5\,\Delta t$ and is the simplest construction of initial CTMs and TMs. The first extension steps (cf figure 3) are performed without renormalization until the dimension of the CTMs exceeds the number m of DMRG states.

As the transfer matrix C_u is only used for the construction of ψ_R^x, which is not needed for computing $\rho_x^{[2]}$, C_u can be omitted completely. If additionally the local Hamiltonian $h_{i,i+1}$ is parity invariant, i.e. $h_{i,i+1} = h_{i+1,i}$, the local transfer matrix τ becomes symmetric. Hence, only the CTMs C_l, C_d and TMs T_{ld}, T_{lu} have to be stored. C_r, T_{rd} and T_{ru} can be reconstructed by mirroring C_l, T_{ld} and T_{lu}.

In order to avoid floating point overflows of the algorithm, it is recommended to rescale all CTMs and TMs

$$C_x \to \frac{C_x}{\|C_x\|} \qquad T_x \to \frac{T_x}{\|T_x\|} \tag{28}$$

where $\|\cdot\|$ is some norm. Note that these rescaling factors have to be considered in the computation of $n(t)$.

All computations were done on Sun Workstations (Ultra Sparc III, 900 MHz). Compared to the old stochastic TMRG [10, 11] the LCTMRG algorithm is tremendously more efficient. Furthermore, as most parts of the program consist of matrix multiplications of CTMs and TMs, the LCTMRG algorithm can easily be paralleled. The CPU time needed for one Trotter step ranges from a few milliseconds for $m = 32$ states up to a couple of seconds for $m = 400$ states. The consumption of computer memory is modest as well, e.g. 10 MB for $m = 32$ up to 200 MB for $m = 400$.

4. Application

4.1. The model

The numerical studies of the present work focus on reaction–diffusion processes (RDP) which are used to model various chemical reactions. We consider a simple RDP with one type of

particle A which exhibits the following reactions:

$$\begin{array}{lll} \text{diffusion:} & A\emptyset \leftrightarrow \emptyset A & (\text{with rate D}) \\ \text{annihilation:} & AA \rightarrow \emptyset\emptyset & (\text{with rate } 2\alpha) \\ \text{coagulation:} & AA \rightarrow \emptyset A,\ A\emptyset & (\text{with rate } \gamma) \\ \text{death:} & \emptyset A,\ A\emptyset \rightarrow \emptyset\emptyset & (\text{with rate } \delta) \\ \text{decoagulation:} & \emptyset A,\ A\emptyset \rightarrow AA & (\text{with rate } \beta). \end{array} \tag{29}$$

This RDP can be expressed by a stochastic Hamiltonian $H = \sum_i h_{i,i+1}$ with local interactions

$$h_{i,i+1} = \begin{pmatrix} 0 & -\delta & -\delta & -2\alpha \\ 0 & D+\delta+\beta & -D & -\gamma \\ 0 & -D & D+\delta+\beta & -\gamma \\ 0 & -\beta & -\beta & 2(\alpha+\gamma) \end{pmatrix}. \tag{30}$$

$h_{i,i+1}$ is parity invariant and the local transfer matrix τ becomes symmetric. Therefore the LCTMRG algorithm simplifies (cf section 3.4).

As an example, we apply the new LCTMRG algorithm to two RDPs, the diffusion–annihilation process and the branch–fusion process. These models have also been chosen by Carlon *et al* [9] to demonstrate the efficiency of the stochastic DMRG algorithm.

The diffusion–annihilation process (DAP)

$$2D = \alpha \qquad \beta = \gamma = \delta = 0 \tag{31}$$

is exactly solvable [17]. For an unbiased initial probability distribution the dynamic evolution of the local density is given by

$$n(t) = \tfrac{1}{2}(I_0(4Dt) + I_1(4Dt))\,\mathrm{e}^{-4Dt} \tag{32}$$

where I_0, I_1 are modified Bessel functions. Thus we can use analytical results to check the numerical precision of the TMRG data. Note that the DAP is critical for all D with an asymptotic behaviour $n(t) \sim t^{-1/2}$.

The branch–fusion process (BFP)

$$D = 2\alpha = \gamma = \delta =: 1 - p \qquad \beta =: p \tag{33}$$

is a simple one-parameter model which exhibits a non-equilibrium phase transition from an active to an absorbing phase. The BFP is not exactly solvable, but Monte Carlo simulations and stochastic DMRG computations [9] are available. The critical behaviour of the BFP falls into the DP universality class where precise data for the critical exponents have been calculated by series expansions [18].

Using the stochastic LCTMRG for both models can demonstrate whether the method is capable of producing reliable results for

- critical and non-critical systems
- systems at phase transition points.

The next subsections present numerical results for the two processes. If not stated differently, all computations were performed with $\Delta t = 0.05$.

4.2. The diffusion–annihilation process

Figure 4 (left) compares LCTMRG calculations with exact data for $D = 0.05$, keeping various numbers of states m. Up to more than $M \sim 10^5$ Trotter steps we obtain highly precise data with a deviation of less than 10^{-5} from the exact results. The inset of figure 4 (left)

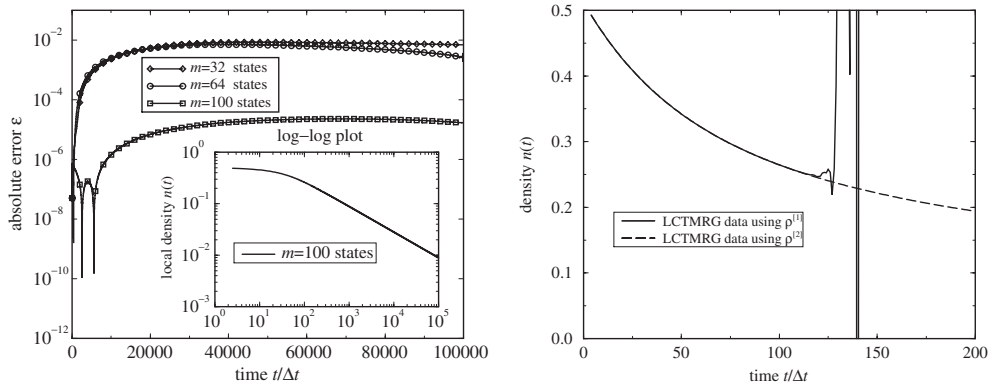

Figure 4. The left figure compares exact data for the DAP with LCTMRG computations by showing the absolute error $\epsilon = |n_{\mathrm{LCTMRG}}(t) - n_{\mathrm{exact}}(t)|$ for $D = 0.05$, keeping $m = 32, 64, 100$ states. The inset plots LCTMRG data for $D = 0.05$ and $m = 100$ in a double-logarithmic plot and shows the algebraic decay. The right figure depicts LCTMRG data for $D = 0.5$, $m = 32$ by using different density matrices $\rho^{[1]}$ and $\rho^{[2]}$.

plots the LCTMRG data in a double-logarithmic plot, which shows that $n(t)$ falls off algebraically.

The high number of Trotter steps M is a considerable improvement on the old stochastic TMRG algorithm [10, 11] by at least *three* orders. Even though the DAP is critical, we observe an extremely stable convergence of the LCTMRG algorithm.

Figure 4 (right) plots numerical data for different density matrices $\rho^{[1]}$ and $\rho^{[2]}$ (cf section 3.3). In all our calculations we observe highly unstable numerics, if the conventional density matrix $\rho^{[1]}$ is used. In the example of figure 4 the convergence of the algorithm breaks down after $M \sim 10^2$ Trotter steps, while $M \sim 10^5$ is possible for $\rho^{[2]}$. Thus the arguments given in section 3.3 can be confirmed numerically: $\rho^{[1]}$ is not an adequate density matrix for the stochastic LCTMRG.

4.3. The branch–fusion process

In this section we focus on the critical phase transition of the BFP at $p_c = 0.84036(1)$ [9]. Figure 5 (left) compares numerical data computed by the LCTMRG algorithm with conventional Monte Carlo simulations. For p sufficiently far away from criticality, we observe a convergence up to more than 10^4 Trotter steps. In the vicinity of the critical point $p \sim p_c$ the convergence becomes worse. Figure 5 (right) plots the logarithmic derivative

$$\mathcal{L}(t) = \frac{\log n(t + \Delta t) - \log n(t)}{\log \Delta t} \tag{34}$$

at the critical point $p \sim p_c$ for $m = 400$ states, which is very sensitive to numerical errors. Up to more than 10^3 Trotter steps the numerics are extremely precise, and one can verify that $n(t)$ switches to an algebraic behaviour. It is also possible to determine the critical exponent α by extrapolating $\mathcal{L}(t \to \infty)$ (cf inset of figure 5 (right)). Thereby, we were able to compute α up to a precision of less than 0.1%:

$$\alpha \approx 0.1600(5) \qquad (\text{literature } \alpha_{\mathrm{lit}} = 0.159\,464(5), [18]). \tag{35}$$

The question arises why the convergence of the LCTMRG at $p \sim p_c$ is two orders less than in the DAP process, yet both models behave critical. We checked various numerical aspects to determine the origin of the worse convergence.

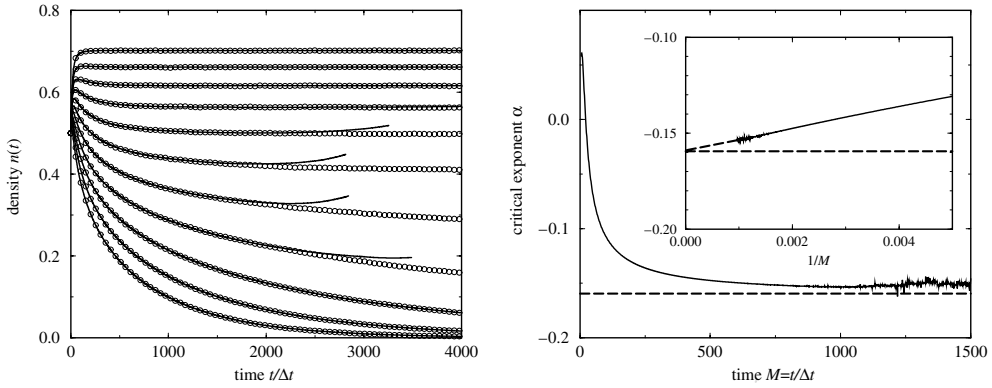

Figure 5. The left figure shows the dynamic evolution of the order parameter $n(t)$ of the BFP for $p = 0.9, \ldots, 0.8$ (in steps of 0.01) keeping $m = 200$ states. For comparison Monte Carlo simulations ($\circ$) are plotted. The right figure plots the logarithmic derivative $\mathcal{L}(t)$ which converges to the critical exponent α. The literature value is plotted by a dashed line. The inset shows $\mathcal{L}(1/t)$ which is used to interpolate the critical exponent α.

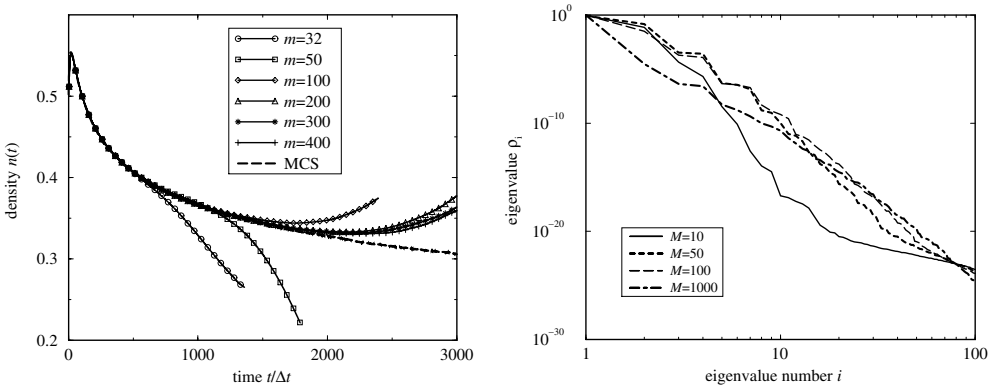

Figure 6. The left figure plots the dynamic evolution of the order parameter $n(t)$ of the BFP at criticality $p \sim p_c$ for various numbers of kept states $m = 32, \ldots, 400$. A MCS is plotted for comparison by a dashed line. On the right one can see the spectrum ρ_i of the density matrix ρ for Trotter steps $M = 10, 50, 100, 1000$ at criticality $p \sim p_c$.

In the BFP it is conspicuous that the quality of the results at $p \sim p_c$ strongly depends on the number of states m that are retained within the LCTMRG algorithm. This is demonstrated in figure 6 (left) which plots numerical computations for various m at $p \sim p_c$. However, it is surprising that so many states m are needed although there is a very strong fall off of the density-matrix eigenvalues ρ_i (cf figure 6 (right)).

As another possibility we check the influence of the size of the Trotter steps Δt on the numerics. The curves of figure 7 (left) belong to various Δt, but are rescaled to $\Delta t = 0.05$ for comparison. Even though finer Trotter decompositions increase the total number of convergent Trotter steps, one cannot improve the accuracy of the data with respect to the absolute time t. If on the other hand Δt becomes too large, the Trotter decomposition itself gets worse and is then responsible for unsatisfactory numerical data.

To estimate the effect of numerical errors caused by floating point inaccuracies we implemented the diagonalization routine for the density matrix alternatively by using higher

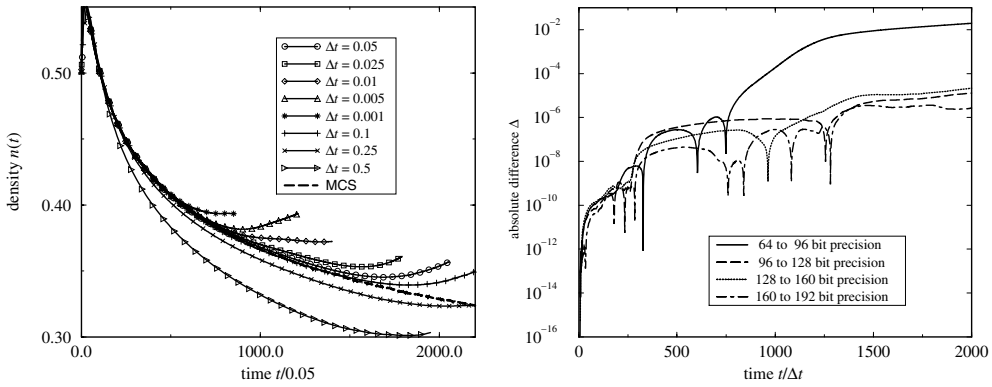

Figure 7. Both plots show the order parameter $n(t)$ of the BFP at criticality $p \sim p_c$, keeping $m = 64$ states. On the left $\Delta t = 0.001 \ldots 0.5$ is varied. The right figure compares data calculated with various floating point precisions (i.e. 64, 96, 128 and 160 bits). The plot shows the differences of numerical data for each precision compared to the next higher one.

mantissa bits. This was technically realized by using the GMP library [19] which allows an arbitrary number of mantissa bits. As shown in figure 7 (right), only a marginal effect on the numerics is observed.

Overall, it remains an open question what exactly is the limiting factor for the worse convergence at the phase transition point $p \sim p_c$ in the BFP. To exclude model specific reasons, we also checked other RDPs, e.g. the contact process. Qualitatively, the same limited convergence near the critical phase transition point is observed.

5. Conclusions and outlook

In the present work, we proposed a new variant of the stochastic TMRG by using corner transfer matrices which we call stochastic light-cone CTMRG (LCTMRG). The LCTMRG algorithm fits genuinely to the specific structure of the triangle classical lattice which evolves from the Trotter–Suzuki decomposition of the stochastic model.

We tested the new algorithm by comparing LCTMRG data with exact results and Monte Carlo simulations of two different reaction–diffusion models. We obtained highly precise numerical results ($\epsilon \sim 10^{-5}$) up to $M \sim 10^5$ Trotter steps, even if the model behaves critical as in the diffusion–annihilation process. Compared to the old stochastic TMRG algorithm [10, 11] with $M \sim 10^2$, this is an enormous increase in the number of reachable Trotter steps of three orders. An important observation is that inherent numerical problems of the old stochastic TMRG algorithm obviously do not appear in our new approach. In the vicinity of a critical phase transition point, exemplified by the branch–fusion model, the convergence gets worse, but is nevertheless sufficient to determine precise results for critical exponents.

Since *within* critical phases a much better convergence has been observed, it remains an open question what exactly causes the reduced convergence at critical phase *boundaries*, which presumably does not originate from purely numerical reasons. Therefore, our future research is concentrated on further modifications and improvements of the LCTMRG algorithm, e.g. the implementation of a finite-size algorithm.

Overall, the numerical investigations show that the new LCTMRG algorithm is a considerable step towards a general and very efficient method for 1D stochastic problems.

Compared to the traditional approach using Monte Carlo simulations, there are two fundamental advantages of the LCTMRG:

- The LCTMRG is not a simulation technique. There is no need to take random numbers and sample averages. The LCTMRG is a numerical renormalization group based on the quantum formalism for stochastic models where averages are directly accessible.
- The algorithm describes the *exact* thermodynamic limit $L \to \infty$ of the stochastic model. Note that here we even have to deal with a *finite* classical 2D system only, due to the simplification from the 'light-cone decoupling'. Thus, there are in principle no finite-size effects as in MCS or stochastic DMRG.

Even if the number of possible time steps, in particular at phase transition points, cannot compete with MCS up to now, we believe that stochastic TMRG algorithms can be an extremely valuable tool for studying 1D stochastic systems. Finally we mention that—as in the case of the CTMRG [20]—a generalization of the LCTMRG to more than one dimension is also imaginable.

Acknowledgments

The work of AK, AS and JZ has been performed within the research program SFB 608 of the *Deutsche Forschungsgemeinschaft*. AK is supported by *Studienstiftung des Deutschen Volkes*. He thanks AG and TN for their warm hospitality at the University of Kobe and the *Kölner Gymnasial- und Stiftungsfonds* for the financial support of this visit.

References

[1] White S R 1992 *Phys. Rev. Lett.* **69** 2863
White S R 1993 *Phys. Rev.* B **48** 10345
[2] Peschel I, Wang X, Kaulke M and Hallberg K (ed) 1998 *Density-Matrix Renormalization* (Heidelberg: Springer)
[3] Nishino T 1995 *J. Phys. Soc. Japan* **64** 3598
[4] Bursill R J, Xiang T and Gehring G A 1996 *J. Phys.: Condens. Matter* **8** L583
Wang X and Xiang T 1997 *Phys. Rev.* B **56** 5061
[5] Trotter H F 1959 *Proc. Am. Math. Soc.* **10** 545
Suzuki M 1985 *Proc. Am. Math. Soc.* **26** 601
[6] Nishino T and Okunishi K 1996 *J. Phys. Soc. Japan* **65** 891
Nishino T and Okunishi K 1997 *J. Phys. Soc. Japan* **66** 3040
[7] Alcaraz F C, Droz M, Henkel M and Rittenberg V 1994 *Ann. Phys., NY* **230** 250
[8] Schütz G M 2000 *Phase Transitions and Critical Phenomena* vol 19 ed C Domb and J Lebowitz (London: Academic)
[9] Carlon E, Henkel M and Schollwöck U 1999 *Eur. Phys. J.* B **12** 99
[10] Kemper A, Schadschneider A and Zittartz J 2001 *J. Phys. A: Math. Gen.* **34** L279
[11] Enss T and Schollwöck U 2001 *J. Phys. A: Math. Gen.* **34** 7769
[12] Hinrichsen H 2000 *Adv. Phys.* **49** 815
[13] de Oliveira S M, de Oliveira P M C and Stauffer D 1999 *Evolution, Money, War and Computers* (Stuttgart: Teubner)
[14] Chowdhury D, Santen L and Schadschneider A 2000 *Phys. Rep.* **329** 199
[15] Marro J and Dickman R 1999 *Nonequilibrium Phase Transitions in Lattice Models* (Cambridge: Cambridge University Press)
[16] Kinzel W 1983 *Ann. Isr. Phys. Soc.* vol 5 (Bristol: Hilger)
Kinzel W 1985 *Z. Phys.* **58** 229
[17] Spouge J L 1988 *Phys. Rev. Lett.* **60** 871
[18] Essam J W, Guttmann A J, Jensen I and Tanlakishani D 1996 *J. Phys. A: Math. Gen.* **29** 1619
[19] GNU multiprecision library (GMP) available from `www.gnu.org`
[20] Nishino T and Okunishi K 1998 *J. Phys. Soc. Japan* **67** 3066